Indian Journal of Fibre & Textile Research
Vol. 50, March 2025, pp. 15-25
DOI: 10.56042/ijftr.v50i1.7189

Development of durable copper-coated ultralight weight nonwoven fabric: Focus on EMI shielding

Aravin Prince Periyasamy[1,2,a] & Jiri Militky[2]

[1]Biomaterial Processing and Products / Textile and Nonwoven Materials,
VTT Technical Research Centre of Finland, Tietotie 4E, Espoo, 021 50 Finland

[2]Department of Material Engineering, Faculty of Textile Engineering,
Technical University of Liberec, Studentska 2, Liberec 461 17, Czech Republic

Received 8 December 2023; revised received and accepted 3 April 2024

This study aims to develop the sol gel technique to enhance the durability of copper coatings on polyester nonwoven (NW) fabric while achieving effective electromagnetic interference (EMI) shielding. FTIR and XRD analyses confirm the successful silanisation of NW fabrics, while SEM imaging reveals uniform silane deposition on the copper-coated NW fabrics. The presence of silane directly impacts EMI shielding capabilities, making these treated NW fabrics highly promising for advanced applications. Durability assessments demonstrate that sol-gel coatings improve mechanical and environmental stability. Washing durability tests show that untreated fabrics lose up to 65% of EMI SE, whereas sol-gel-treated fabrics retain their shielding properties. In conclusion, silane coating on conductive NW fabrics exhibits enhanced durability, effectively maintaining copper adhesion and EMI shielding under mechanical stress, washing, and chemical exposure.

Keywords: Air permeability, Areal density, Conductive textiles, Copper-coated, EMI Shielding, Sol-gel coating

1 Introduction

Currently, there exists a significant presence of electromagnetic interference (EMI) pollution, which has been extensively identified, stemming from the rapid growth of the technologies in the communications field and its associated devices[1–3]. EMI has been identified as a significant contributor to various health ailments, including but not limited to symptoms of fatigue, anxiety, sleep disturbances, mood disorders, migraines, haematological malignancies such as leukaemia, cancer; furthermore, it has been observed to impact DNA integrity through the disruption of electrical pulses[4-5]. The generation of high-frequency electromagnetic radiation and EMI may indicate potential health hazards for both humans and other organisms[6–8]. For instance, prolonged radiation exposure can lead to various biological effects, primarily attributed to the thermal effects on tissues, resulting in tissue damage[9,10]. The research and development of conductive textiles have garnered significant attention due to their multifunctionality[11–14], particularly their ability to provide efficient electromagnetic interference shielding effectiveness (EMI SE). Conductive textiles exhibit favourable attributes such as low weight, flexibility, and requisite mechanical properties, making them viable contenders for substituting traditional metallic materials[15-16]. Traditionally, the utilisation of metal fibres or metal wire integrated fabric for EMI shielding necessitates the inclusion of a greater quantity of metal wire or fibre to achieve the desired level of EMI SE, resulting in increased weight and reduced flexibility[17]. Meanwhile, it is worth noting that materials composed of metals or coated with metals exhibit shielding ranges ranging from 40 dB to 100 dB, which can be considered significantly high.

In most cases, the effectiveness of EMI shielding is primarily determined by the type and concentration of metal deposition on the textile materials. However, it is important to acknowledge that there exist two significant constraints linked to textiles coated with metals. The inadequate affinity between metal and textile materials results in diminished durability of the coated metals on the textile surface. For example, copper-coated textiles possess the potential for undergoing an oxidation process when subjected to diverse environmental elements such as moisture, saltwater, and overall atmospheric conditions[18].

[a]Corresponding author.
E-mail: aravinprincep@gmail.com

Consequently, oxidation diminishes the material's ability to maintain its electrical conductivity, efficacy in providing protection against EMI shielding, and thermal conductivity. In certain instances, the process of protecting copper from oxidation through silver electroplating has been documented[19]. However, the presence of a silver coating on the surface of the fabric prevents it from being classified as a pure copper coating. The fabric's high cost and formidable safety measures further contribute to its limited accessibility. Therefore, the fabric that is produced demonstrates a decrease in comfort properties because of the presence of a dense layer caused by silver electroplating.

In this study, we propose a sol-gel coating approach to enhance the durability of copper-coated nonwoven (NW) fabrics. To improve adhesion and stability, the copper-coated NW fabrics were treated with two silanes, each applied at distinct molar ratios. Despite the growing body of research on conductive textiles, only a few studies have assessed the durability of copper-coated fabrics under conditions such as abrasion, washing, and chemical exposure[20–22]. This article represents the first investigation into the silane combination and its impact on EMI shielding, abrasion resistance, washing durability, and chemical stability of copper-coated nonwoven fabrics.

2 Materials and Methods

2.1 Materials

In this study, 100% polyester filament cross-laminated ultralightweight nonwoven (NW) fabric, commonly referred to as Milife, was supplied by JX Nippon ANCI Corporation, Japan. To facilitate copper plating, the Milife fabric was subjected to an activation process aimed at elevating the surface tension above 50 mN m^{-1} by hydrolysis in alkalis or plasmatic preparation. The metallisation of the Milife NW fabric was performed via autocatalytic activation, followed by immersion in a strong alkali bath at 24±2°C (Vecernk s.r.o)[23–27]. Microscopic imaging revealed a distinct bilayer structure of the Milife fabric, with copper particles deposited on the surface. Laboratory-grade reagents were procured from Sigma Aldrich, Prague, Czech Republic. Table 1 presents a comprehensive overview of the essential geometric characteristics of the fabric before and after silanisation treatment.

2.2 Sol-gel Synthesis and Coating

For the silanisation process, two different silane precursors, Triethoxy(phenyl)silane (PhTES) and (3-Aminopropyl)triethoxysilane (APTES), were employed in varying molar (M) ratios (Table 1). The sols were prepared by combining the precursors with a catalyst (Triacetoxyvinyl silane) and a solvent (99% ethanol (EtOH)). The catalyst played a dual role: facilitating the reaction and acting as a third precursor. Triacetoxyvinyl silane exhibited a gradual release of acetic acid, thereby preventing rapid hydrolysis. The sol-gel synthesis was conducted by mixing PhTES and APTES with the catalyst and EtOH solvent in specific silane, catalyst, water, and solvent proportions at 32:1:100:320 M, respectively[24,25,28,29]. After this preparation, copper-coated Milife NW fabrics were subjected to dip-coating process. The coated NW fabrics were then dried under standard atmospheric conditions and then cured at 120°C for 7 min. The sol-gel-coated fabric samples were conditioned for 48 h before conducting EMI SE measurements to ensure thorough stabilisation of the silica matrices.

2.3 Testing of Coated Fabric

2.3.1 SEM, Energy Dispersive X-ray Analysis and FTIR

The surface morphology of the NW fabrics was examined using a TS5130 Vega-Tescan scanning electron microscope under a working distance of 2.5 mm and voltage of 20 kV). Chemical composition analysis was conducted via energy dispersive X-ray (EDX) spectroscopy using an Oxford Inca 200 detector attached to the SEM. Attenuated Total Reflectance Fourier Transform Infrared (ATR-FTIR) spectra of cMi and pMi samples were recorded using a Nicolet Spectrometer (iS10) with a ZnSe ATR crystal, spanning a spectral range of 4000-500 cm^{-1}.

2.3.2 X-ray Diffraction

The influence of silanisation on the crystalline structure was analysed using a Shimadzu X-ray diffractometer operating at 40 kV and 30 mA with

Table 1 — Geometrical characteristics of pMi and cMi NW fabrics

Fabric code	Description
pMi	Un-plated Milife NW fabric
cMi	Copper-plated Milife NW fabric
cMi + P0A100	cMi coated with silane (PhTES:APTES=0:100)
cMi + P10A90	cMi coated with silane (PhTES:APTES=10:90)
cMi + P20A80	cMi coated with silane (PhTES:APTES=20:80)
cMi + P30A70	cMi coated with silane (PhTES:APTES=30:70)
cMi + P40A60	cMi coated with silane (PhTES:APTES=40:60)
cMi + P50A50	cMi coated with silane (PhTES:APTES=50:50)
cMi + P60A40	cMi coated with silane (PhTES:APTES=60:40)
cMi + P70A30	cMi coated with silane (PhTES:APTES=70:30)
cMi + P80A20	cMi coated with silane (PhTES:APTES=80:20)
cMi + P90A10	cMi coated with silane (PhTES:APTES=90:10)
cMi + P100A0	cMi coated with silane (PhTES:APTES=100:0)

Cu Kα radiation. X-ray Diffraction (XRD) patterns were interpreted with reference to the Joint Committee on Powder Diffraction Standards (JCPDS) card No. 00-050-2275.

2.3.3 EMI SE Measurement

The EMI shielding effectiveness (EMI SE) of copper-plated Milife NW fabrics was assessed using an EMI SE tester across a frequency range of 30 MHz to 1.5 GHz following the ASTM D4935-10 standard[30]. To ensure consistency, testing was conducted at a controlled room temperature of 21°C and relative humidity of 55%.

The EMI SE values were computed using equation 1, where S_{21} denotes the forward transmission coefficient[26].

$$SE(S21) = -10\log\left(\frac{P_1}{P_2}\right) = 10\log\left(\frac{P_2}{P_1}\right) \quad \text{... (1)}$$

where P_2 and P_1 represent the received powers in the presence and absence of the fabric, respectively. The input reflection coefficient was using Eq. (2):

$$S_{11} = 10\log\left(\frac{P_3}{P_1}\right) \quad \text{... (2)}$$

where P_3 is the power received in the presence of reflections. Each measurement was conducted in five replicates at different locations, and mean values were used for subsequent computations.

2.3.4 Abrasion Resistance and Washing Durability

Abrasion resistance was tested using a Martindale Abrasion Tester in accordance with ISO 12947-1:1998, applying a pressure of 9 kPa for 10, 20, 30, 40, and 50 cycles. Changes in EMI SE values before and after the abrasion test were recorded. Washing durability was assessed using the AATCC 61-1A method, which involved washing it without using steel balls. The tests were done for 45 min at 40°C with a Testex launder-o-meter, followed by rinsing with water twice and then drying. EMI SE was measured before and after washing.

2.3.5 Chemical Stability

The chemical stability of the pMi and cMi fabrics, both before and after the application of the sol-gel process, was evaluated using the immersion test. NW fabrics were submerged for 72 h in various solutions, including water, boiling water, 1M NaCl, 1M NaOH, 1M HCl, 1M CH_3COOH, and EtOH. EMI SE loss was recorded post-immersion.

2.3.6 Physical Properties

The thickness gauge tester was used to measure the fabric thickness according to the ASTM D1777 standard. Area density was calculated using the ASTM D3776-07 standard. ISO 9237 was used to measure the air permeability in Textest FX 3300. The mass add-on percentage of the sol-gel-coated cMi NW fabric was determined by comparing the mass of the fabric before and after coating.

3 Results and Discussion

3.1 Surface Morphology of pMi & cMi Fabric

SEM images of conductive Milife (cMi) and pristine Milife (pMi) NW fabrics are shown in Fig. 1. The

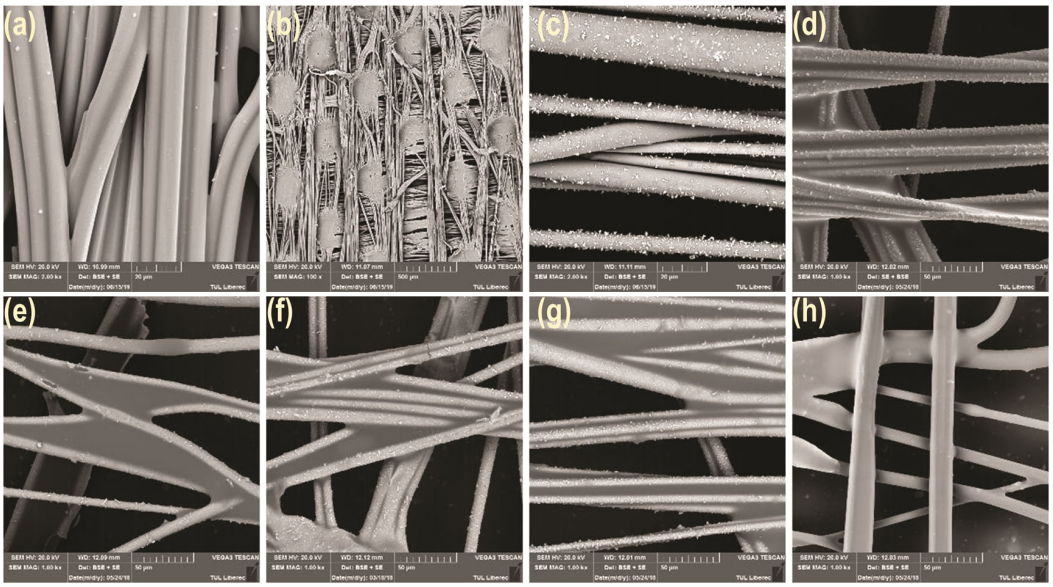

Fig. 1 — Surface view of (a) pMi, (b) cMi, (c) copper deposition on cMi, and influence of sol-gel treatment on cMi (d) cMi+P0A100, (e) cMi+P30A70, (f) cMi+P50A50, (g) cMi+P70A300, and (h) cMi+P100A0

surface of the pMi fabric exhibits a smooth texture with no extraneous material deposits [Figure 1 (a)]. Fig. 1 (b) displays the thermal binding locations on the surface of cMi fabric, revealing a rough texture indicative of copper deposition. Observations indicate that the deposited copper is predominantly located on the fibre surfaces rather than occupying the inter-fibre spaces. This can be attributed to the thinness of the copper coating layer, which enhances air permeability and, consequently, comfort properties. Additionally, the copper coating is found to be nearly uniform, with a range of 0.47 to 0.60 g/m^2. This corresponds to a GSM (grams per square metre) range of 10.47 to 10.60 g/m^2, indicating the lightweight characteristic of the fabricated NW fabrics[16].

The sol-gel treatment forms a uniform layer on the Milife fabric, stabilising the copper coating, as observed in the SEM images [Fig. 1 (d) – (h)]. The impact of varying silane ratios on the surface roughness of cMi fabrics is evident. A higher ratio of PhTES resulted in a thicker coating on the copper plating [Fig. 1 (h)], effectively concealing the copper on the surface. SEM images reveal a correlation between increased PhTES ratios and smoother cMi fibre surfaces, and it has the lowest surface roughness due to the inclusion of a cyclic ring, resulting in a robust three-dimensional silica network on the fibre materials coated with copper[24]. However, the thickness of this film is contingent upon the specific silane type and its corresponding viscosity[31–33]. The attenuation of electromagnetic waves caused by repeated reflections and scattering is amplified by the deposition of copper on NW fabrics. Moreover, post-silanisation copper deposition forms a thin coating with a significant specific surface area, which is crucial for enhancing EMI shielding efficiency.

Further, EDX mapping and analysis reveal the spatial distribution and elemental identification of copper particles on the cMi fabrics. Figure 2 shows the uniform dispersion of copper (Cu), nickel (Ni), titanium (Ti), carbon (C), and oxygen (O). EDX confirms the existence of copper on the surface of cMi NW textiles, with a weight percentage of 12.8% for copper and 1.2% for nickel [Fig. 2 (g)].

3.2 FTIR Characterisation

ATR-FTIR spectroscopy was employed to analyse the effects of sol-gel treatment and copper deposition on the NW fabrics. Figure 3 (a) reveals characteristic peaks at 1014 cm^{-1}, 1706 cm^{-1}, 1096 cm^{-1}, and 1247 cm^{-1}, corresponding to C=O stretching vibrations in ester groups, indicating deformation in CH_2 and CH_3 groups of the polyester fabric. The CH_3 group is responsible for the typical absorption peaks around 2985 cm^{-1} in polyester. The spectral region of 1300-1000 cm^{-1} is similar to C=O stretching vibrations found in ester groups in polyester. Distinct peaks at 780 cm^{-1} and 820 cm^{-1} indicate the presence of Si-CH bonds resulting from the sol-gel treatment, consistently observed across all silane ratios. A novel Si-O-Si stretching vibration was detected in sol-gel-treated cMi fabric, coinciding with the polyester C-O absorption band at approximately 1100 cm^{-1}[34, 35]. Additionally, a peak at 505 cm^{-1} corresponds to the deformation and bending vibration of the Si-O-Si framework. In the present study, copper-coated Milife NW fabrics exhibit additional peaks between 1713 cm^{-1} to 1627 cm^{-1} and

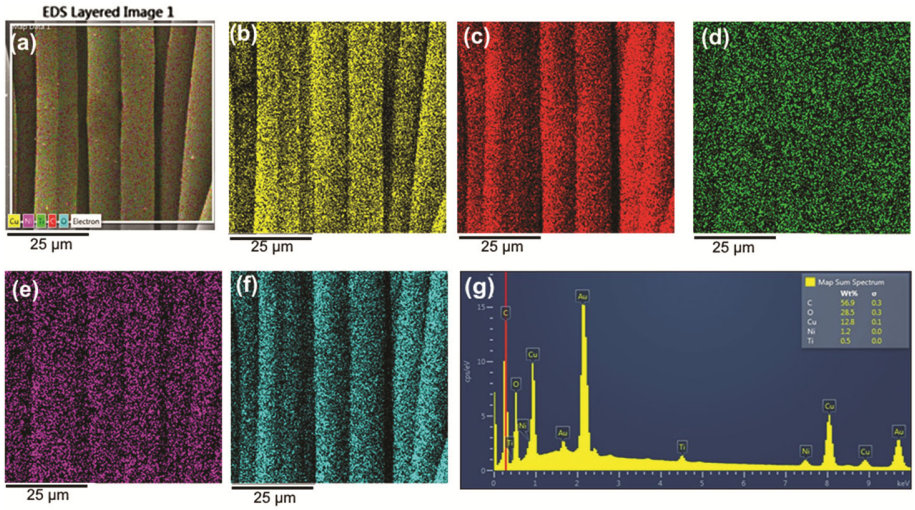

Fig. 2 — EDX mapping (a) microscopic image, (b) carbon, (c) oxygen, (d) copper, (e) nickel, (f) titanium, and (g) spectra of cMi NW fabrics

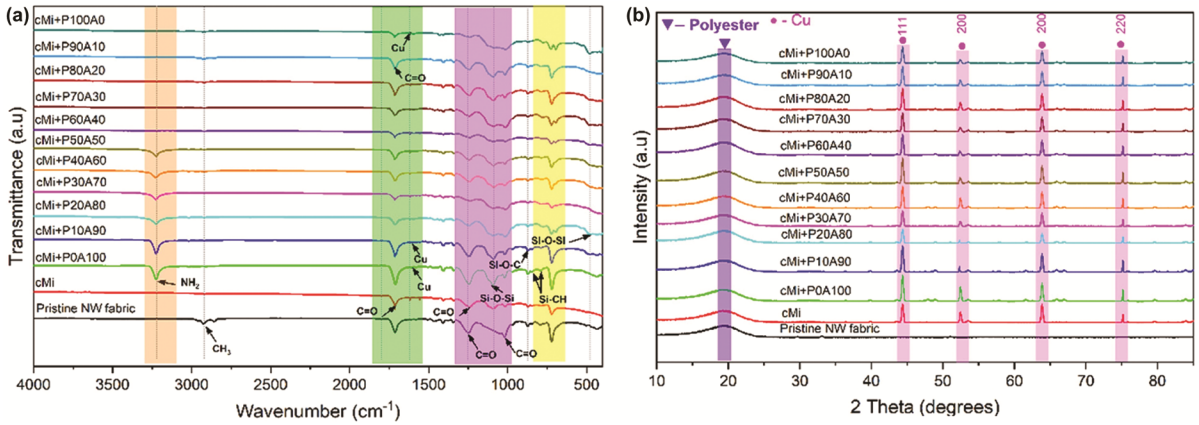

Fig. 3 — (a) FTIR spectra and (b) XRD patterns of pMi and cMi NW fabrics

1555 cm^{-1} to 1425 cm^{-1}, confirming a significant level of integration between the NW fabrics and copper[24,36].

3.3 *XRD* Characterisation

Figure 3 (b) presents XRD patterns for the pMi, cMi and silane-treated cMi NW fabrics. As anticipated, the X-ray diffraction pattern of pMi does not exhibit any discernible peaks corresponding to copper. Based on JCPDS card number 00-050-2275, pMi fabric exhibits a prominent peak at 20.0° C[37]. These peaks can be attributed to the presence of crystal planes corresponding to the polyester structure, specifically the (011) planes[38]. Copper deposition significantly influences the crystalline structure of Milife fabrics. XRD analysis of cMi reveals additional diffraction peaks at 2θ = 44.3°, 52.3°, 63.8° and 75.2°, corresponding to different crystal planes (111), (200), and (220) of copper deposition, as shown by the JCPDS card number 85-1326[39–41]. These peaks confirm successful copper deposition. Post-silanisation, no substantial difference in sol-gel ratios was observed, as evidenced by the unchanged XRD patterns. Sol-gel-coated cMi textiles show distinct peaks at around 48.2 and 57.21, corresponding to Si(220) and Si(311) planes, respectively. However, the intensity of the diffraction peak is comparatively weaker than that of copper. Some silane ratios (cMi+P20A80, cMi+P30A70, and cMi+P40A60) show reduced intensity at 2θ=44.2°, though the NW structure remained unchanged [Fig. 3 (b)]. The PhTES compound contains a phenyl group included as a precursor, which lacks a prominent peak, similar to APTES.

3.4 Sol-Gel Treatment and EMI Shielding

The coaxial transmission line technique, in accordance with ASTM standards, was used to evaluate the EMI SE of pMi, cMi, and sol-gel-treated cMi fabrics (Fig. 4). The NW fabrics were tested across a frequency range of 30 MHz to 1.5 GHz with SE values expressed in decibels (dB). This study chose EMI SE at 1.5 GHz due to its relevance to numerous electronic devices (e.g., mobile phones, GPS, Wi-Fi routers).

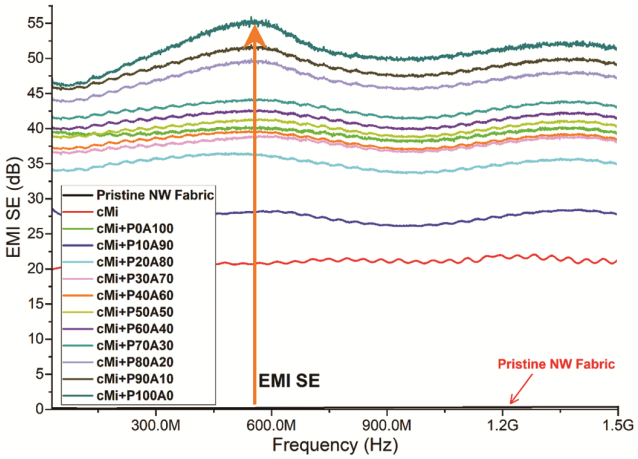

Fig. 4 — Effect of sol-gel treatment on EMI SE of pMi and cMi NW fabrics

Sol-gel treatment significantly enhances EMI SE compared to untreated cMi NW fabric. The shielding performance depends on the silane ratio, with the best outcomes obtained at a higher PhTES ratio. The absence of copper in pMi leads to inadequate attenuation of the electromagnetic field, resulting in a limited shielding capability (~EMI SE >1). The values exhibit an inverse relationship with frequency. It is widely recognised that Copper alone is insufficient to achieve high EMI SE.

The cMi + P100A0 fabric exhibits the highest EMI SE of 47 dB at the lowest frequency (30 MHz) and 51 dB at 1.5 GHz, with a peak SE of 56 dB at 0.55 GHz.

Comparatively, the SE of cMi + P100A0 is nearly twice that of untreated cMi NW fabric, demonstrating the effectiveness of sol-gel treatment. The shielding efficiency values of cMi + P0A100 (APTES higher ratio) also show notable outcomes, achieving over 37 dB at 30 MHz and increasing to 39 dB at 1.5 GHz. PhTES-rich silanes yielded higher EMI SE values than APTES due to their chemical structure, characterised by an aromatic ring. This structural feature facilitates the absorption of electromagnetic radiation through robust bonding interactions inside the cyclic ring. The carbon-carbon, carbon-hydrogen, and benzene rings are situated within a single torus, hence enhancing the shielding efficiency of the cMi + P100A0 fabric. As an example, it can be observed that the phenyl group consists of three conjugated π bonds. Compounds that include π electrons exhibit pronounced absorptions towards EM radiation, potentially enhancing the SE of composite materials as a whole. Moreover, the presence of phenyl groups leads to generating anion radicals, which convert to C-centred radicals through protonation, further enhancing EM radiation absorption[42–44]. On the contrary, APTES lacks the necessary π electrons, limiting its interaction with EM radiation.

Conductive textiles are classified into five categories based on EMI shielding applications, ranging from moderate to exceptional protection. General applications include casual clothing, maternity wear, and consumer electronics protection, while professional applications involve shielding garments for electronic industries and medical equipment. Based on these classifications, the developed fabrics are recommended for professional electromagnetic shielding applications, particularly in protective clothing[16,24].

3.5 Durability Measurement

Stability and durability are crucial for wearable conductive materials to ensure their practical utility. Conductive textiles, particularly those fabricated with copper or other metal coatings, typically tend to detach from the fibre surface when subjected to mechanical stresses such as wearing, rubbing, or washing. This detachment can be attributed to the relatively weak contact between the conductive materials and the surface of the fibres.

3.5.1 Abrasion Resistance

Abrasion resistance refers to the ability of fabrics to withstand surface wear caused by direct contact and rubbing. Figure 5(a) displays the abrasion resistance of cMi NW fabrics. The Milife NW fabrics were analysed over 75 cycles, with damage and hole formation observed. To prevent excessive damage, the test was subsequently reduced to 50 cycles.

Applying a sol-gel coating on cMi fabrics significantly enhances the abrasion resistance. Additionally, this sol-gel layer serves as a protective barrier, as reflected in changes in EMI SE values after abrasion cycles [Fig. 5(b)]. PhTES to APTES's molar ratio substantially impacts the decrease in EMI SE values, confirming that the silane molar ratio directly affects abrasion resistance. EMI SE values are measured before and after testing. Initial EMI SE values for NW fabrics with no abrasion are 39 dB and 51 dB for cMi + P0A100 and cMi + P100A0, respectively. After 50 abrasion cycles, these values decrease to 26 dB and 30 dB, respectively, with a greater loss associated with a higher PhTES ratio, demonstrating the influence of sol-gel chemistry on surface properties.

Notably, cMi + P30A70 exhibits the lowest abrasion resistance. This can be attributed to the

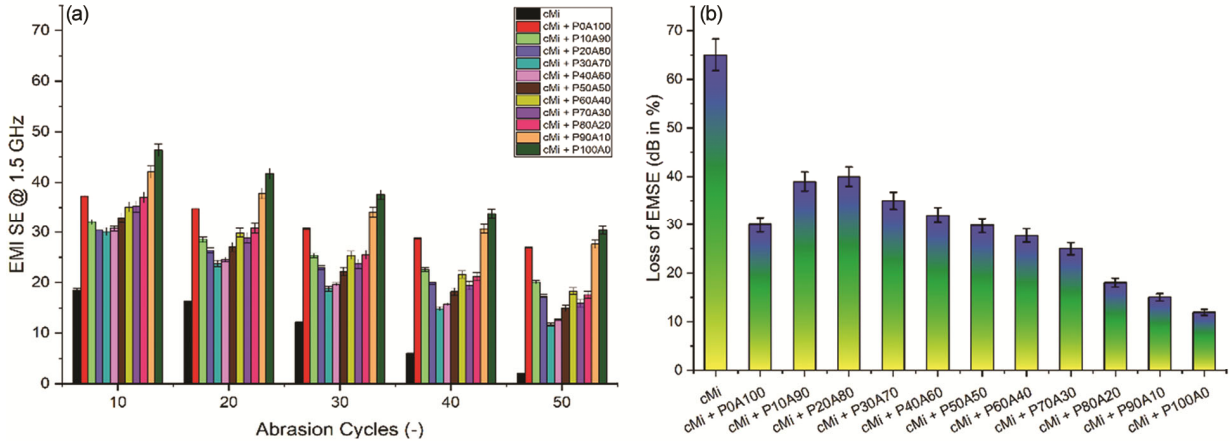

Fig. 5 — Influence of sol-gel treatment on (a) abrasion resistance of cMi fabric, and (b) loss of EMI SE values

specific concentration and interaction of PhTES and APTES, which influence the viscosity of the sol-gel coating. A predominance of APTES may result in a thinner coating layer. Although it would be necessary to measure the viscosity and coating thickness to confirm this, they are beyond the scope of the current study. Future research should explore the influence of sol-gel viscosity on coating thickness.

The morphological analysis (Fig. 6) confirms that the sol-gel-treated Milife fabric maintains its protective silica gel coating even after extended abrasion with minimal deformation. In contrast, fabrics without a sol-gel coating exhibit noticeable disruption of copper particles [Fig. 6 (g)]. These findings are consistent with EMI SE values, further confirming the protective effect of sol-gel treatment. A higher PhTES content (e.g., cMi + P100A0) leads to greater protection on the surface with Cu particles [Fig. 6 (a)]. The observed phenomenon can be attributed to the formation of a three-dimensional network structure and the presence of phenyl rings within the silica sol.

3.5.2 Washing Resistance

To assess washing durability, AATCC standard washing tests are conducted on copper-plated NW fabrics with different PhTES:APTES silane ratios. EMI SE values are measured before and after washing [Fig. 5 (b)]. The application of sol-gel treatment provides protection to copper during simulated domestic washing processes, with minimal impact on its properties. Notably, fabrics treated with cMi + P100A0 exhibit the least EMI SE reduction, indicating that increasing the PhTES ratio enhances protection. This is due to the ability of PhTES to prevent hydrolysis and bond degradation, which otherwise lead to copper loss. Following five standard washing cycles, fabrics without sol-gel coating experience a 65% EMI SE loss, whereas coated fabrics exhibit significantly lower reductions depending on the silane ratio.

The microscopy analysis [Fig. 7] reveals that sol-gel treatment protects against friction caused by contact with the washing machine drum. Fabrics without sol-gel treatment suffer severe copper layer degradation, leading to reduced EMI shielding and increased oxidation risk [Fig. 7 (h)].

3.5.3 Chemical Stability

Chemical resistance is critical for the longevity of copper-plated NW fabrics. A 72-hour immersion test is conducted in various chemical environments. EMI SE values are measured after 72 h [Fig. 8 (a)]. Among tested solutions, 1M NaOH has the most significant impact on EMI SE values, followed by 1M HCl, 1M NaCl, and 1M CH3COOH. Although copper is

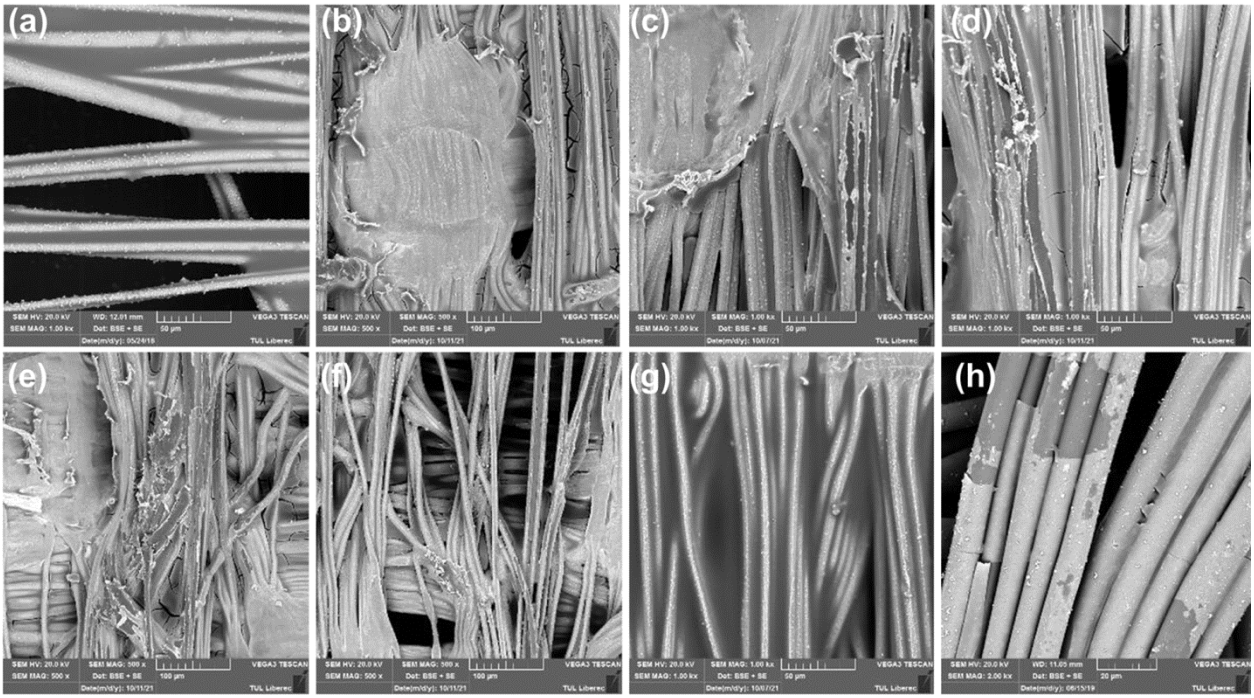

Fig. 6 — Morphological analysis of 50 cycles abraded (a) cMi + P100A0 (b) cMi + P90A10, (c)cMi + P70A30, (d) cMi + P50A50, (e) cMi + P30A70, (f) cMi + P10A90, (g) cMi + P0A100, and (h) cMi

generally resistant to corrosion in acidic and alkaline conditions, extreme environments can disrupt copper's physical interaction with the fabric[45], leading to reduced dispersion and increased copper particle loss, which can be environmentally harmful.

This reduction in dispersion generally results in a decrease in the values of EMI SE. When exposed to an acidic environment, copper is unable to displace hydrogen in hydrochloric acid (HCl) to form copper (II) chloride ($CuCl_2$). This lack of reaction between copper and HCl might be attributed to copper's greater reduction potential than hydrogen. Nevertheless, the reaction between copper and acids is heavily influenced by the presence of oxygen. Even when exposed to non-oxidising acids such as HCl, the formation of $CuCl_2$ or copper chloride ($Cu_2(OH)_3Cl$) can still occur. The rate of oxidative corrosion on the surface of copper is accelerated in the presence of

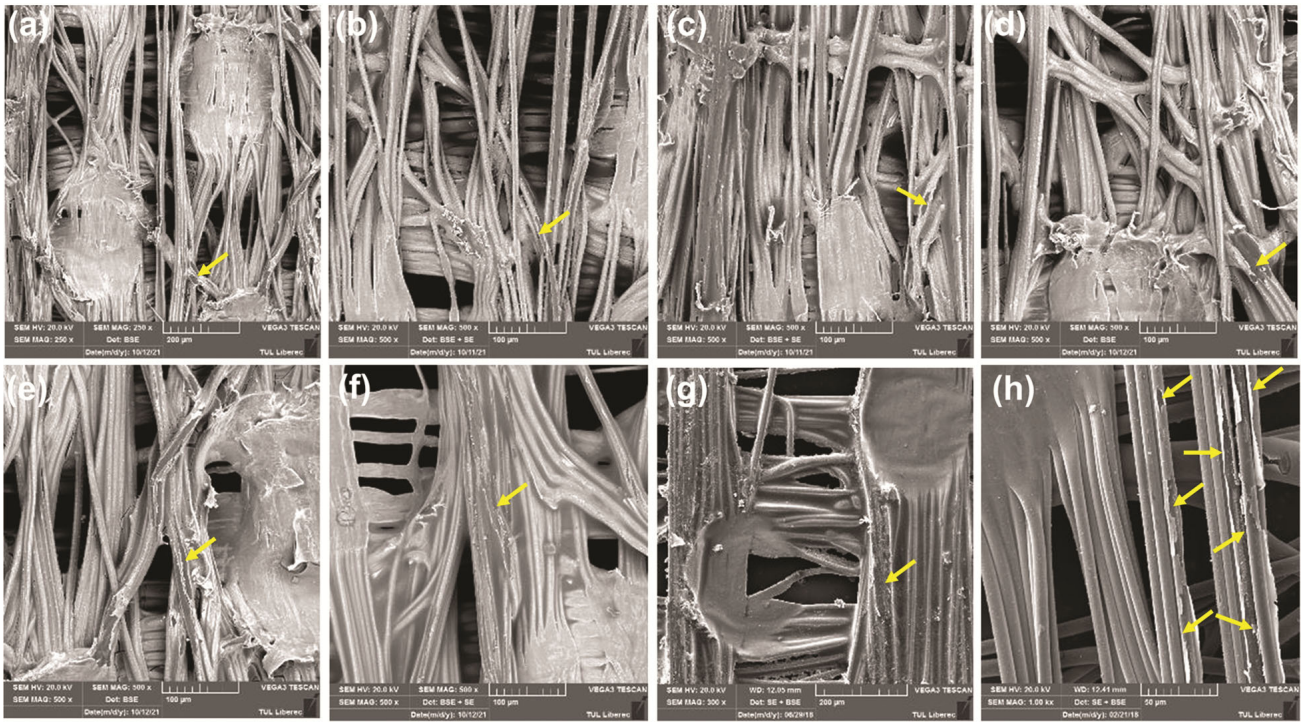

Fig. 7 — Microscopical changes after washing in (a) cMi + P100A0, (b) cMi + P90A10, (c) cMi + P70A30, (d) cMi + P50A50, (e) cMi + P30A70, (f) cMi + P10A90, (g) cMi + P0A100, and (h) cMi

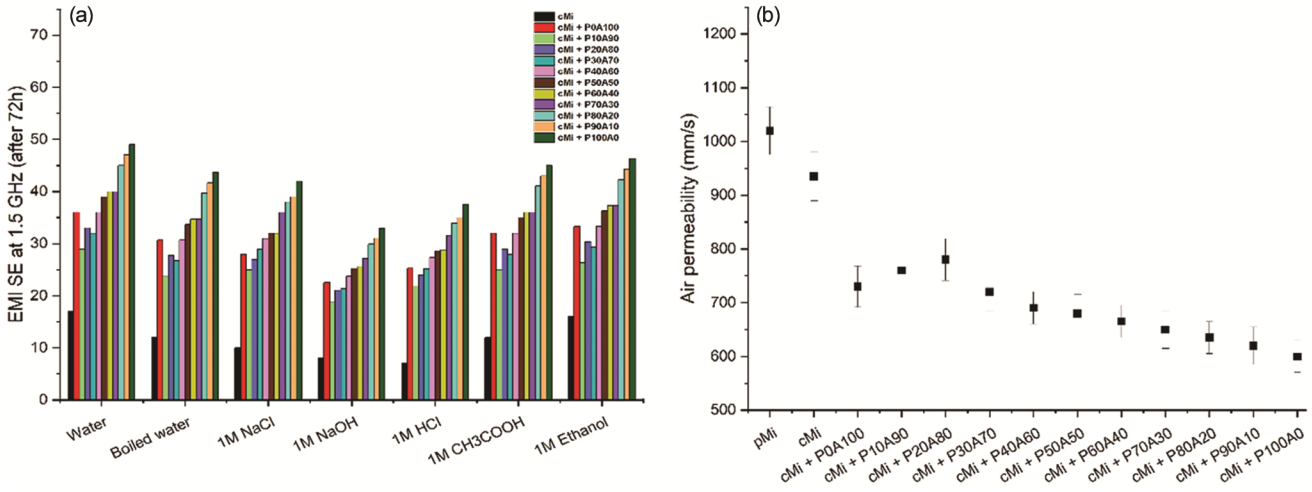

Fig. 8 — (a) Influence of different chemical environments on the EMI SE at 1.5 GHz values and (b) influence of sol-gel process on the air permeability of cMi NW fabrics

oxygen or other oxidising substances[45]. The corrosion of copper by alkali is a gradual phenomenon, although detectable. Nevertheless, the oxidation process persists when the metal is exposed to a diluted NaOH solution. This activity becomes more noticeable when the metal is in simultaneous contact with both air and water.

Acetic acid tends to react with fabrics that contain copper, resulting in the formation of copper (II) acetate[45]. The formation of a free radical occurs when copper, acetic acid, and atmospheric oxygen combine, initiating an electrochemical corrosion process — the possible hydrolysis of sol-gel in extremely acidic and alkaline environments[46–48]. The rate of hydrolysis is affected by both the pH level and the individual organo- and silicon-functional groups[49]. Several factors can affect the interaction between sol-gel and inorganic particles. The factors encompassed in this study are the intrinsic pH of the silane compound, the isoelectric point of the particle under investigation, the water-to-silane ratio employed, the pH level of the reaction media, and the nature of the dispersion medium. The hydrolysis rate is observed to be higher at extreme pH levels, specifically above 11 and below 2, compared to the sol-gel's inherent pH level, offering the most favourable silanes stability.

3.5 Physical Properties

3.5.1 Air Permeability

Figure 8 (b) reveals the air permeability of pMi, cPi, and sol-gel-coated NW fabrics. Typically, air permeability decreases following the copper plating process, which aligns with expectations due to copper deposition on the porous structure. In general, sol-gel treatment reduces air permeability, typically by 20–30%, depending on the specific silane ratio. Notably, a greater reduction in air permeability is observed when the PhTES ratio is higher. The deposition of a rigid PhTES layer on the fibre surface likely contributes to this decline. However, in contrast to previous research[50], the sol-gel-treated cMi NW fabric in this study exhibits an air permeability exceeding 600 mm/s, thereby maintaining good breathability.

3.5.2 Thickness and Areal Density

Table 2 summarises key physical parameters, including thickness, density, porosity, areal mass, and mass add-on. Sol-gel treatment significantly influences density porosity percentage and areal mass, while its impact on mass add-on percentage is relatively minor. No substantial variation in thickness is observed with an increasing APTES/PhTES ratio. However, the rigid structure of the silica network often leads to an increase in fabric thickness in samples treated with a higher proportion of PhTES. The areal density undergoes alterations when additional materials are applied to a substrate. In this study, sol-gel coated NW fabrics demonstrate greater areal density compared to the cMi NW fabrics.

The sol-gel coating exhibits significant degradation in extreme chemical conditions, as observed through SEM imaging (Fig. 9). It is observed that the sol-gel coating exhibits significant peeling in certain areas [Fig. 9 (e) – (g), (n) – (q)], leading to a subsequent decrease in EMI SE values (Fig. 9). Among all tested coatings, cMi + P100A0, which has the highest PhTES content, demonstrates the best resistance to acidic, alkaline, and organic solvents.

Table 2 — Physical characteristics of pMi and cMi NW fabrics

Fabric code	Thickness, mm	Density porosity, %	Areal mass, g/m^2	Mass add-on, %
pMi	0.040 ±0.026	79 ± 3.25	11.4 ± 0.252	-
cMi	0.063 ±0.034	81 ± 3.68	16.6 ± 1.145	-
cMi + P0A100	0.067 ± 0.017*	87 ± 3.88*	17.9 ± 0.747*	7.6
cMi + P10A90	0.067 ± 0.023*	85 ± 3.72*	17.8 ± 0.711*	7.2
cMi + P20A80	0.066 ± 0.017*	85 ± 3.73*	17.6 ± 0.734*	7.1
cMi + P30A70	0.066 ± 0.019*	86 ± 2.36*	17.7 ± 0.565*	7.2
cMi + P40A60	0.065 ± 0.021*	86 ± 2.25*	17.8 ± 0.344*	7.3
cMi + P50A50	0.066 ± 0.022*	86 ± 3.35*	17.8 ± 0.987*	7.4
cMi + P60A40	0.066 ± 0.021*	87 ± 2.68*	17.9 ± 0.765*	7.6
cMi + P70A30	0.067 ± 0.021*	87 ± 2.67*	18.1 ± 0.723*	7.8
cMi + P80A20	0.068 ± 0.023*	87 ± 2.66*	18.2 ± 0.788*	7.9
cMi + P90A10	0.068 ± 0.022*	87 ± 3.27*	18.3 ± 0.567*	8.1
cMi + P100A0	0.068 ± 0.025*	88 ± 2.99*	18.4 ± 0.724*	8.3

*Denotes standard deviation

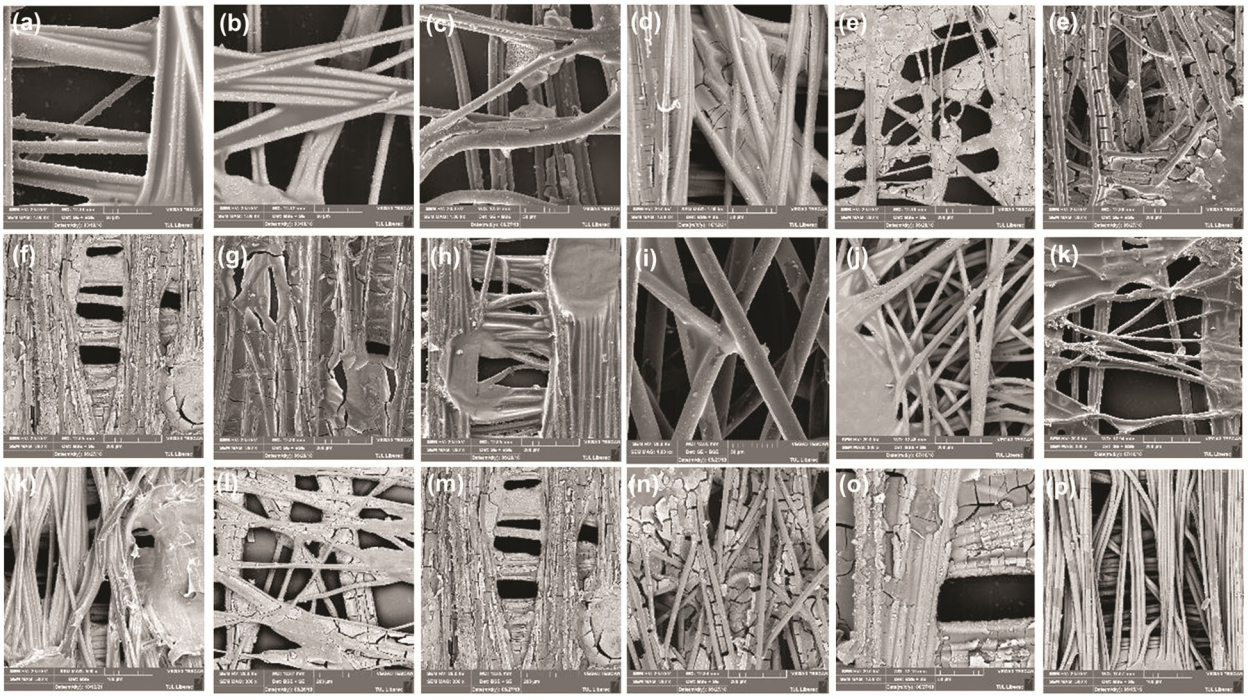

Fig. 9 — SEM images of (a) cMi fabric, (b-h) cMi + P100A0 after 72 *h* immersion of in (b) with water, (c) boiling water, (d) 1M NaCl, (e) 1M NaOH, (f) 1M HCl, (g) 1M CH_3COOH and (h) EtOH; (i) cMi fabric, (j-p) cMi + P0A100 after 72 *h* immersion in (j) water, (k) boiling water, (l) 1M NaCl, (m) 1M NaOH, (n) 1M HCl, (o) 1M CH_3COOH, and (p) EtOH

4 Conclusion

This study evaluates the stability of Cu-coated NW fabrics in terms of their physical, chemical, and mechanical properties. A sol-gel coating incorporating silane is successfully applied to Cu-coated NW fabrics without compromising their core characteristics. The findings indicate that Cu stabilisation on cMi NW fabrics enhances their potential for smart textile applications, particularly in EMI shielding. The sol-gel-treated cMi NW fabrics exhibit significantly higher EMI SE values attributed to the chemical interactions of the silanes used in the treatment process. Applying sol-gel coating improves the EMI SE of cMi NW textiles, while SEM images confirm the uniform silane deposition on the copper-coated NW fabrics. These images also demonstrate the impact of abrasion, washing, and exposure to various chemical environments on the integrity of the silane coating. In general, the application of silane coating on conductive NW textiles augments their durability, significantly improving abrasion and washing resistance, as well as their ability to withstand diverse chemical conditions. Additionally, these coated textiles remain lightweight, porous, and sufficiently air-permeable, making them suitable for various protective textile applications, including fibre-sandwiched structures.

Acknowledgement

This work is supported by the Ministry of Education, Youth and Sports of the Czech Republic and the European Union - European Structural and Investment Funds in the frames of Operational Programme Research, Development and Education through the project Hybrid Materials for Hierarchical Structures (HyHi, Reg. No. CZ.02.1.01 /0.0/0.0/16_019/0000843).

References

1 Geetha S, Kumar K K S, Rao C R K, Vijayan M & Trivedi D C, *J Appl Polym Sci*, 112 (2009) 2073.
2 Riaz S, Naz S, Younus A, Javid A, Akram S, Nosheen A & Ashraf M, *Colloids Surf A Physicochem Eng Asp*, 650 (2022) 129486.
3 Cassauwers T, Is 5G bad for your health? It's complicated, say researchers, 2019.
4 Panagopoulos D J, *Mutat Res Rev Mutat Res*, 781 (2019) 53.
5 De-Iuliis G N, Newey R J, King B V & Aitken R J, *PLoS One*, 8 (2009).
6 Buckus R, Strukčinskienė B, Raistenskis J, Stukas R, Šidlauskienė A & Čerkauskienė R, *Int J Environ Res Public Health*, 14 (2017) 244.
7 Deji S, Nishizawa K, *Health Phys*, 89 (2005) 224.
8 Kizilay A, Ozturan O, Erdem T, Tayyar Kalcioglu M & Cem Miman M, *Auris Nasus Larynx,* 30 (2003) 239.
9 Jagetia G C, *Environ Res*, 212 (2022) 113321.
10 Ahlbom I C, Cardis E, Green A, Linet M, Savitz D & Swerdlow A, *Environ Health Perspect*, 109 (2001) 911.

11 Lee J, Kwon H, Seo J, Shin S, Koo J H & Pang C, *Adv Materials*, 27 (2015) 2433.
12 Lv J, Jeerapan I, Tehrani F, Yin L, Silva-Lopez C A & Jang J H, *Energy Environ Sci,* 414 (2018) 2478.
13 Pakdel E, Naebe M, Sun L & Wang X, *ACS Appl Mater Interfaces,* 35 (2019) 13039.
14 Wei Q, Xiao X, Hou D, Ye H & Huang F, *Surf Coat Technol,* 202 (2008) 2535.
15 Kelvin Fu K, Padbury R, Toprakci O, Dirican M & Zhang X, *Woodhead Publishing*; (2018) 305.
16 Yang K, Periyasamy AP, Venkataraman M, Militky J, Kremenakova D &Vecernik J, *Polymers*, 12 (2020) 2029.
17 Lu G, Li X & Jiang H, *Compos Sci Tech,* 56 (1996)193.
18 Tao L, Lee J & Akinwande D, *Nanotechnology and Microelectronics: Materials, Processing, Measurement, and Phenomena*, 29 (2011) 06FG07.
19 Cao X G & Zhang H Y, *Elec Mater Let*, 8 (2012) 467.
20 Šaravanja B, Pušić T, Malarić K & Hursa Šajatović A, *TEKSTILEC,* 14 (2021) 25.
21 Jiang S, Miao D, Li A, Guo R & Shang S, *Fibr Polym*, 17 (2016) 1397.
22 Zhang X, Miao D, Ning X, Cai M, Tian Y & Zhao H, *Vacuum,* 164 (2019) 205.
23 Periyasamy A P, Yang K, Xiong X, Venkatraman M & Militky J, *Textile Bioengineering and Informatics Symposium Proceedings 2019 - 12th Textile Bioengineering and Informatics Symposium*, Suzhou, China, (2019) 67.
24 Periyasamy A P, Yang K, Xiong X, Venkataraman M, Militky J & Mishra R, *Mater Chem Phys,* 239 (2020) 122008.
25 Periyasamy AP, Venkataraman M, Militky J, *J Mater Sci*, 57 (2022) 20780.
26 Hu S, Wang D, Periyasamy A P, Kremenakova D, Militky J & Tunak M, *Polym*, 13 (2021) 4176.
27 Venkataraman M, Yang K, Periyasamy AP, Xiong X & Militky J, Nanocon; *10th Anniversary International Conference on Nanomaterials - Research & Application* Brno, Czech Republic.
28 Periyasamy A P, Venkataraman M, Kremenakova D, Militky J & Zhou Y, *Materials,* 14 (2020) 1838.
29 Periyasamy A P, Vikova M & Vik M, *J Text Inst,* 111 (2020) 808.
30 ASTM D 4935-10:2010: Standard Test Method for Measuring the Electromagnetic Effectiveness of Planar Materials. West Conshohocken, PA; 2010.
31 Guglielmi M & Zenezini S, *J Non Cryst Solids,* 121 (1990) 303.
32 Klein L, Handbook of sol-gel science and technology: processing, characterization, and applications, *Springer Publications*, 2018.
33 Gallo T A & Klein L, *J Non Cryst Solids*, 82 (1986) 198.
34 Qian X, Song L, Bihe Y, Yu B, Shi Y & Hu Y, *Mater Chem Phys,* 143 (2014) 1243.
35 Tran T P T, Bénézet J C & Bergeret A, *Ind Crops Prod*, 58 (2014) 111.
36 Rani K V, Sarma B & Sarma A, *Vacuum*, 146 (2017) 206.
37 Xu W, Yuan X, Wei A, Feng Q & Wei Q, *Surface Engineering*, 2 (2018) 838.
38 Zhao Z, Zhou J, Fan T, Li L, Liu Z & Liu Y, *Mater Chem Phys,* 203 (2018) 89.
39 Wei N, Cui H, Song Q, Zhang L, Song X & Wang K, *Appl Catal B,*198 (2016) 83.
40 Shao W, Li G, Zhu P, Zhang Y, Ouyang Q & Sun R, *J of Mater Sci: Materials in Electronics,* 11 (2018) 4432.
41 Zheng J, Lin Z, Liu W, Wang L, Zhao S & Yang H, *J Mater Chem B* (2014) 6207.
42 Robert J Woods & Alexei K P, *Applied Radiation Chemistry: Radiation Processing* (1993).
43 Radziszewski J G, Nimlos M R & Ellison G B, *J Am Chem Soc, 1* (1996) 7400.
44 Jin H, Giri B R, Liu D & Farooq A, *Proceedings of the Combustion Institute*, 17 (2021) 919.
45 DeMeo S, *J Chem Educ*, 22 (1997) 844.
46 Okhrimenko D, Budi A, Ceccato M, Cárdenas M, Johansson D B & Lybye D, *ACS Appl Mater Interfaces,* 115 (2017) 8344.
47 Arkles B, Pan Y, Larson G L & Singh M, *A Euro J,* (2014) 9442.
48 Noronha V T, Sousa F A, Souza Filho A G, Silva C A, Cunha F A & Koo H, *J Phys Chem C,* 96 (2017) 11300.
49 Bergna H & Roberts W, Colloidal Silica: Fundamentals and Applications, 2005.
50 Sheng J, Zhang M, Xu Y, Yu J & Ding B, *ACS Appl Mater Interfaces,* 94 (2016) 27218.